International Journal of Heat and Mass Transfer 158 (2020) 119947

Contents lists available at ScienceDirect

International Journal of Heat and Mass Transfer

journal homepage: www.elsevier.com/locate/hmt

Experimental investigation of laminar flow and heat transfer characteristics in square minichannels with twisted tapes

Zhenfei Feng[a,b,*], Xin Ai[a], Peilin Wu[a], Qingyu Lin[a,b], Zuqiang Huang[c,*]

[a] School of Mechanical Engineering, Guangxi University, Nanning 530004, China
[b] Guangxi Key Laboratory of Petrochemical Resource Processing and Process Intensification Technology, Guangxi University, Nanning 530004, China
[c] School of Chemistry and Chemical Engineering, Guangxi University, Nanning 530004, China

ARTICLE INFO

Article history:
Received 1 January 2020
Revised 3 May 2020
Accepted 10 May 2020

Keywords:
Heat transfer enhancement
Overall thermal performance
Minichannel
Twisted tape
Laminar flow

ABSTRACT

The flow and heat transfer characteristics of distilled water in a minichannel heat sink (MCHS) fitted with twisted tapes under laminar flow are investigated experimentally in present study. Nine twisted tapes with lengths of $L_t = 50$ mm, 100 mm and 150 mm, and twist ratios of $Y = 3$, 4, and 5 are employed as inserts. The results show that average heat transfer coefficient (h_{ave}), pressure drop per unit length (ΔP_{pul}) and thermal enhancement factor (η) increase with the decrease in twist ratio or/and the increase in twisted tape length. The heat transfer enhancement factor ($h_{ave}/h_{ave,0}$, where subscript 0 denotes plain MCHS) and the pressure drop increasing factor ($\Delta P_{pul}/\Delta P_{pul,0}$) are in the ranges of 1.29–2.49 and 1.68–4.72, respectively. The average values of η for each MCHS with twisted tape are in a range of 1.09–1.46. The full-length ($L_t = 150$ mm) twisted tape with $Y = 3$ yields the best heat transfer rate, the highest flow resistance and the best overall thermal performance compared to other eight twisted tapes. In addition, the empirical correlations for h_{ave} and ΔP_{pul} are developed based on the experimental results. The predicted h_{ave} and ΔP_{pul} are within ±5% and ±6% deviation, respectively, compared to the experimental data.

1. Introduction

To pursue smaller and more lightweight packaging, the miniaturization of modern electronic and power components is inevitable, leading to rapid increase in heat dissipation during these components working. This is driving the development of more effective cooling solutions to maintain acceptable component temperature and preserve component reliability [1]. A widely and promisingly adopted solution is to use single-phase micro/minichannel heat sinks due to its advantages of high heat dissipation efficiency, compact structure, low power consumption and low coolant consumption [2,3]. Thus, more and more researchers have studied the techniques of heat transfer enhancement in single-phase micro/minichannel heat sink to further enhance its cooling capacity. In these researches, the passive techniques of heat transfer enhancement are widely studied by researchers because these techniques do not require extra power compared to active heat transfer technique.

Among the passive techniques, using enhanced working fluid in microchannel heat sinks have attracted more and more attention in the recent years due to this solution without changing the heat sink structure. Nanofluid is a kind of enhanced working fluid containing nanoparticles made of high thermal conductivity material (e.g. metal, metal oxides and carbon). A number of investigators, such as Ding et al. [4], Xu et al. [5], and Saeed et al. [6], have found that the heat transfer performance were improved using nanofluid in mini/microchannel heat sinks. However, Rimbault et al. [7] reported that CuO-water nanofluid with 0.24 vol% and 1.03 vol% concentration yielded a slight heat transfer enhancement in a microchannel heat sink, but the nanofluid with 4.5 vol% concentration deteriorated heat transfer performance. This is possibly because the nanofluid with high concentration produces obviously clustering of nanoparticles, thereby resulting in deposition of nanoparticles in the microchannel, even blockage of the microchannel in severe cases. This also implies that the nanofluid is not suitable for heat transfer enhancement in the microchannel heat sink from the viewpoint of practical application [8].

Using the improved channel structure is also an important way in passive techniques of heat transfer enhancement. Improving micro/minichannel structure in the heat sink renders the fluid flow field and temperature field to change, thereby enhancing the heat transfer performance. Khoshvaght-Aliabadi et al. [9] found that this solution was more effective than using the nanofluid from

* Corresponding authors.
E-mail addresses: zffeng@gxu.edu.cn (Z. Feng), huangzq@gxu.edu.cn (Z. Huang).

https://doi.org/10.1016/j.ijheatmasstransfer.2020.119947
0017-9310/

Nomenclature

A	cross-sectional area of flow channel
A_{chs}	cross-sectional area of total minichannels
A_t	top planform area of heat sink
c_p	specific heat at constant pressure
D_h	hydraulic diameter of minichannel
$D_{h,sp}$	hydraulic diameter of shallow plenum
D_t	twisted tape width
f	friction factor
H_{ch}	minichannel height
H_R	distance between resistance temperature detector (RTD) and minichannel bottom wall
H_t	axial distance of twisted tape rotated by 180°
h_{ave}	average heat transfer coefficient
k_f	thermal conductivity of fluid
k_s	thermal conductivity of solid
L_{ch}	minichannel length
L_{sp}	length of shallow plenum
L_t	twisted tape length
LR	tape-length ratio, $LR=L_t/L_{ch}$
m	fin parameter
$\dot{m}$	mass flow rate
N_{ch}	number of minichannels
Nu	Nusselt number
Nu_x	local Nusselt number
Po	Poiseuille number
Pr	Prandtl number
ΔP	pressure drop
ΔP_c	inlet contraction pressure loss
ΔP_{ch}	pressure drop of minichannel
ΔP_e	outlet expansion pressure loss
ΔP_{ip}	pressure drop of inlet plenum
ΔP_{op}	pressure drop of outlet plenum
ΔP_{pul}	pressure drop per unit length
ΔP_{tot}	total pressure
$\dot{Q}$	heat input to the fluid across minichannel
q	base heat flux
Re	Reynolds number
T_f	fluid temperature
T_{in}	fluid temperature at inlet
T_{out}	fluid temperature at outlet
T_R	temperature measured by RTD
T_w	temperature of minichannel bottom wall
t	twisted tape thickness
u	velocity
$\dot{V}$	volumetric flow rate
W_{ch}	minichannel height
W_{fin}	width of fin between two adjacent minichannels
W_s	width of heat sink top platform
x	axial distance to minichannel inlet
x^*	dimensionless axial distance
Y	twist ratio, $Y=H_t/D_t$

Greek symbols

α	aspect ratio of rectangular channel, $\alpha \leq 1$
η	thermal enhancement factor
η_{fin}	fin efficiency
μ	dynamic viscosity
ρ	density

Subscripts

0	plain minichannel
ave	average
ch	minichannel
c	inlet contraction
e	outlet expansion
f	fluid
fin	fin
idp	inlet deep plenum
in	minichannel inlet
ip	inlet plenum
isp	inlet shallow plenum
k	inlet shallow plenum (isp) or outlet shallow plenum (osp)
m	mean
n	location number of resistance temperature detector
odp	outlet deep plenum
op	outlet plenum
osp	outlet shallow plenum
out	minichannel outlet
R	resistance temperature detector (RTD)
s	solid, sink
t	top planform of heat sink, twisted tape
tot	total
w	bottom wall
x	coordinate along flow direction

the thermal point of view. Additionally, the stability and reliability of this solution were better than that of using the nanofluid from a practical point of view [9]. Therefore, many researchers have applied this solution to enhance heat transfer performance for the micro/minichannel heat sink in recent years, e.g. Refs. [10-12]. From these studies, it is found that the mechanisms of heat transfer enhancement for using the improved micro/minichannel structure can be concluded as the following three points: (1) the improved channel structure extends the convective heat transfer area; (2) the improved channel structure induces the interruption and redevelopment of hydraulic and thermal boundary layers; (3) the improved channel structure generates vortex/swirl flow and chaotic advection, which can enhance the hot and cold fluid mixing, disturb the development of hydraulic and thermal boundary layers, and increase residence time of fluid, thus their effect of heat transfer enhancement is very remarkable. Vortex/swirl flow can be generated by the swirl/vortex flow devices, which are also important passive heat transfer enhancement methods. More details on passive methods using swirl/vortex flow devices can be found in a review by Sheikholeslami et al. [13].

Twisted tape, as an effective swirl flow device, has been widely employed in the heat exchanger, solar water heater, cooling device, and so on. Because twisted tape has many advantages, such as easy fabrication, convenience mounting, and low cost [14], it always attracts many attention and has been investigated extensively by scholars and engineers. Especially, the researchers had conducted numerous investigations on the modified, twin or multiple twisted tapes in recent years. Abdolbaqi et al. [15] examined turbulent heat transfer in a flat tube fitted with twin twisted tapes, and showed that heat transfer rates in flat tube with twin counter twisted tapes are around 22.5% and 61% higher than those with the twin co-twisted tapes and plain flat tube, respectively. Man et al. [16] reported that a dual-pipe heat exchanger with alternation of clockwise and counterclockwise twisted tape (ACCT tape) performed better heat transfer performance as compared to that with the typical twisted tape, and the full-length ACCT tape obtained the maximum value (1.42) of performance evaluation criteria (PEC). Hong et al. [17] showed that the tube equipped with overlapped multiple twisted tapes performed superior heat transfer rate as compared to the plain tube, and the maximum value of PEC was about 1.08.

He et al. [18] found experimentally that the heat transfer enhancement in the tube with cross hollow twisted tape inserts under laminar flow was better than that under turbulent flow, and the values of PEC were in the range of 0.87 to 0.98. Liu et al. [19] investigated numerically the enhancement performance of laminar convective heat transfer with the coaxial cross twisted tapes. They showed that the coaxial cross twisted tape increased the Nusselt number by 151–195% compared to the traditional twisted tape, and its maximum value of PEC reached 1.92. Abolarin et al. [20] experimentally studied the heat transfer characteristics of peripheral u-cut twisted tapes and ring inserts in the transitional flow regime, and concluded that increasing depth ratio of peripheral u-cut twisted tape and decreasing space ratio of ring enhanced prominently the heat transfer performance. Zhang et al. [21,22] investigated experimentally the overall thermal performance of perforated and unperforated self-rotating twisted tapes. They found that the thermal performance factors of perforated and unperforated self-rotating twisted tapes ranged from 0.862 to 1.101, and from 0.863 to 1.03, respectively. Chu et al. [23] experimentally found that the twisted tape having obtuse V-cut configuration improved pronouncedly Nusselt number and friction factor compared to the successive twisted tape, but it yielded the highest PEC of 1.18–1.23 in the test range. Bhuiya et al. [24] conducted an experimental investigation on thermal performance characteristics of a tube heat exchanger with perforated triple twisted tape. They found that perforated triple twisted tape yielded thermal enhancement efficiency of 1.13-1.5. Hong et al. [25] numerically studied thermal-hydraulic performances in a sinusoidal rib tube with multiple twisted tapes. They showed that the PEC obtained by single, twin, triple and quadruple twisted tapes were in the ranges of 1.35–1.49, 1.16–1.42, 1.06–1.33 and 1.00–1.25, respectively. Recently, using traditional or modified twisted tape as a turbulator, Sheikholeslami et al. [26-31] investigated heat transfer, flow, exergy loss and entropy generation of nanofluid in the heat exchanger tube.

According to the aforementioned literature survey, these researches focused on the macro-scale heat exchanger channel with twisted tape, and there was a lack of research on micro/mini-scale channel with twisted tape. Especially, no article was tried to investigate experimentally the effect of twisted tape on the heat transfer and flow characteristics in micro/minichannels. Also, Feng et al. [3] reported that wire coil inserts enhanced the heat transfer performance in the microchannel heat sink with enhancement factor of 1.2–1.8, and the values of PEC for all cases ranged from 1.08 to 1.51. This means that the enhancement technique for twisted tape inserts is also suitable for improving heat transfer performance in the micro/minichannel heat sink. However, the effects of twisted tape on heat transfer enhancement and pressure drop are not understood in micro/minichannels. Furthermore, a micro/minichannel heat exchanger has been widely used in various applications in recent years. Enhancing heat transfer performance in the micro/minichannel heat exchanger is beneficial to energy conservation and emission reduction. Thus, the investigation of flow and heat transfer characteristics in micro/minichannels fitted with twisted tape inserts have a great significance to further enhance heat transfer performance in micro/minichannels.

From the above analysis, it is very necessary to explore the effect of twisted tape on thermal-hydraulic characteristics in micro/minichannels. This motivates current authors to conduct this research. In this research, experimental investigation has been carried out to find the effects of twist ratio and length of twisted tape on heat transfer coefficient, pressure drop, and overall thermal performance in a minichannel heat sink, where distilled water is used as working fluid. In addition, empirical correlations for heat transfer coefficient and pressure drop per unit length are developed based on the experimental data. This research will extend application of twisted tape inserts to the micro/mini-scale heat transfer field. Also, the results will provide a theoretical reference in the design of micro/minichannel heat exchanger equipped with twisted tape inserts.

2. Experimental methods

2.1. Test module

The construction of test module is illustrated in Fig. 1(a), which is modified based on that of our previous study [32]. Its main component is an oxygen-free copper heat sink having a 150-mm long by 25-mm wide top surface. The top surface of the heat sink contains 8 of 2×2 mm^2 parallel minichannels. The reason for choosing minichannel in present work is because the minichannel not only can be capable to absorb high heat flux but also requires less pressure drop as compared to microchannel. Moreover, such minichannel is benefit to assembly of twisted tape. At a distance of 5 mm under the bottom wall of these minichannels, five shielded platinum resistance temperature detectors (RTDs) are inserted along the center line of the heat sink to measure the stream-wise wall temperature distribution. The locations of these RTDs are 11 mm, 43 mm, 75 mm, 107 mm and 139 mm, respectively, from the minichannel inlet position, as indicated in Fig. 1(a). Eight oxygen-free copper twisted tapes are embedded into the minichannels. Their geometric dimensions are depicted in Fig. 1(a) and (b). The thickness (t) and width (D_t) of the twisted tape are 0.15 mm and 2 mm, respectively. The twist ratio of the twisted tape (Y) is defined as the ratio of the axial distance (H_t) of the twisted tape rotated by 180° to the width of the twisted tape, $Y=H_t/D_t$. The tape-length ratio (LR) is defined as the ratio of twisted tape length (L_t) to the minichannel length (L_{ch}), $LR=L_t/L_{ch}$, where $L_{ch}=150$ mm. Nine types of twisted tape are produced to study the effects of tape-length ratio and twist ratio on heat transfer and flow characteristics in the minichannels, as shown in Fig. 1(b). Their lengths are 50 mm, 100 mm and 150 mm (LR=1/3, 2/3, 1). Because twisted tape with too small twist ratio is difficult to fabricate for the present work, and twisted tape with too large twist ratio can't generate enough swirl intensity to enhance heat transfer significantly, twist ratios selected in present work are 3, 4 and 5 based on the study by Saha et al. [33]. The head ends for nine twisted tapes are positioned at the inlet of minichannel. The tops of the minichannels are closed off by a transparent Pyrex glass cover plate, which also provides optical access to the fluid flow inside the minichannels.

The heat sink is embedded into a rectangular through hole of an insulating housing made from Telfon plastic, and then it is fixed by screws. The housing has inlet and outlet plenums, and each plenum contains a shallow plenum and a deep plenum to ensure uniform flow distribution [34]. Each deep plenum contains a pressure port to connect differential pressure transducer for measurement of pressure drop between inlet and outlet. Furthermore, two RTDs are set at these deep plenums to measure the inlet and outlet temperatures, respectively.

The heat sink bottom surface contacts the top surface of a heating block made from oxygen-free copper. Silver thermal compound is utilized in the interface between both surfaces to diminish contact thermal resistance. The heating block is heated by seven cartridge heaters with the maximum total power of 1400 W. The total power of these heaters is adjusted by a single 0–250 VAC variac and measured by a digital wattmeter. Four fiberglass insulating blocks are used to support and insulate the heating block. A top stainless steel cover brace and a bottom insulating block press tightly the multiple layers of test module together with the aid of stainless steel bolts and screws, as shown in Fig. 1(a). The test module assembly is wrapped by thermal insulation cotton to ensure insulation and minimize heat loss.

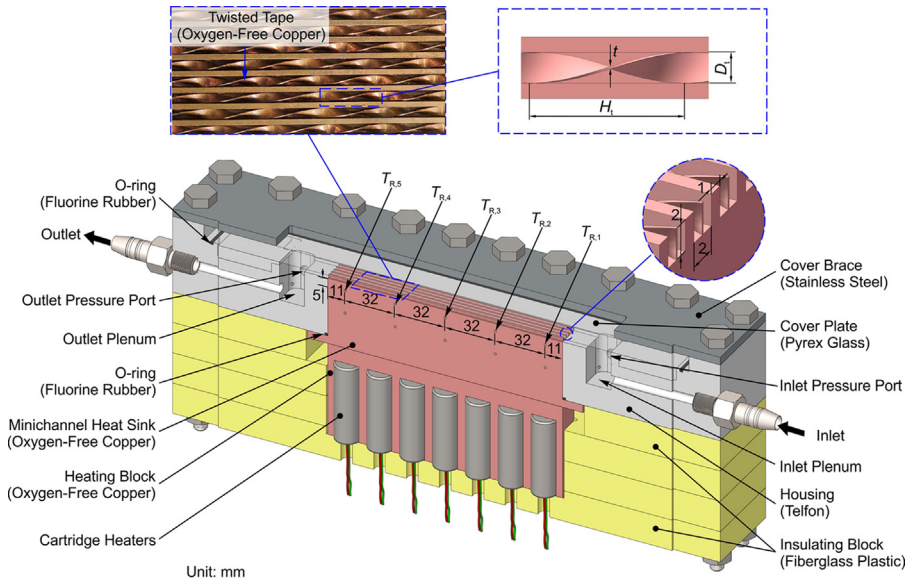

(a)

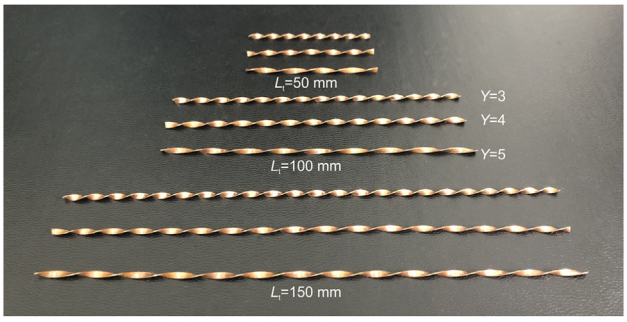

(b)

Fig. 1. (a) Test module construction. (b) Photo of nine types of twisted type.

2.2. Experimental loop

A schematic diagram of the experimental flow loop is shown in Fig. 2(a), which is divided into two loops, a test loop and a cooling loop. The working fluid in the test loop and cooling loop are distilled water and cooling water, respectively. To avoid disturbance of non-condensable gases on the test results, the working fluid is fully degassed by vigorous boiling in the test loop's reservoir for about one hour previous to each test run. Degassed fluid is circulated within the test loop using centrifugal pump, as same as the experimental setups of Khoshvaght-Aliabadi and Sahamiyan [35] and Ho et al. [36]. Such pump can generate enough pressure to driver the fluid to pass through the test module stably. Exiting pump, the fluid is divided into two portions. One portion flows through a by-pass valve and then returns to the reservoir. Another portion passes successively a filter, a rotameter, a constant temperature water bath, the test module, a heat exchanger, and finally flows back to reservoir. The test module is connected to the test loop via two silicone tubes, and the differential pressure transducer is also connected to test module by silicone tube. This is beneficial to flow stability in the test module during test running. The flow rate in the test loop is regulated using the by-pass valve or the control valve of the rotameter. The inlet temperature of fluid into the test module is adjusted by the constant temperature bath. Fluid absorbing heat from test module is cooled down by the liquid-to-liquid heat exchanger. Fig. 2(b) shows the pressure drop fluctuation in the minichannels with and without twisted tape. It is found that the amplitude of pressure drop fluctuation is quite small. Thus the pulsation dampener is not used in present flow loop.

2.3. Operating conditions and measurement accuracies

In the present work, the volumetric flow rates are varied from 0.36 to 0.76 L/min, corresponding to Reynolds numbers between 419 and 884 for a single plain minichannel. This means laminar flow in the minichannel. Sheikholeslami et al. [13] concluded that twisted tape inserts perform better thermal performance in laminar flow than turbulent flow. The inlet fluid temperature is maintained at 25°C during test run. Temperature measurements throughout the test module are achieved using RTDs. Each RTD is calibrated in a constant temperature water bath. After this calibration, a maximum error of ±0.1 °C is achieved for each RTD. The differential pressure transducer for measurement of pressure drop between inlet and outlet has an accuracy of ±0.25%. The rotameter with an accuracy of ±2.5% is used to measure the volumetric flow rate of working fluid. The digital wattmeter for the heat input measurement yields an accuracy of ±0.5%. All the temperatures and pressure drop between inlet and outlet in the test module are collected by two Advantech data acquisition modules (ADAM 6217). Table 1 summarizes the accuracy of measuring instruments.

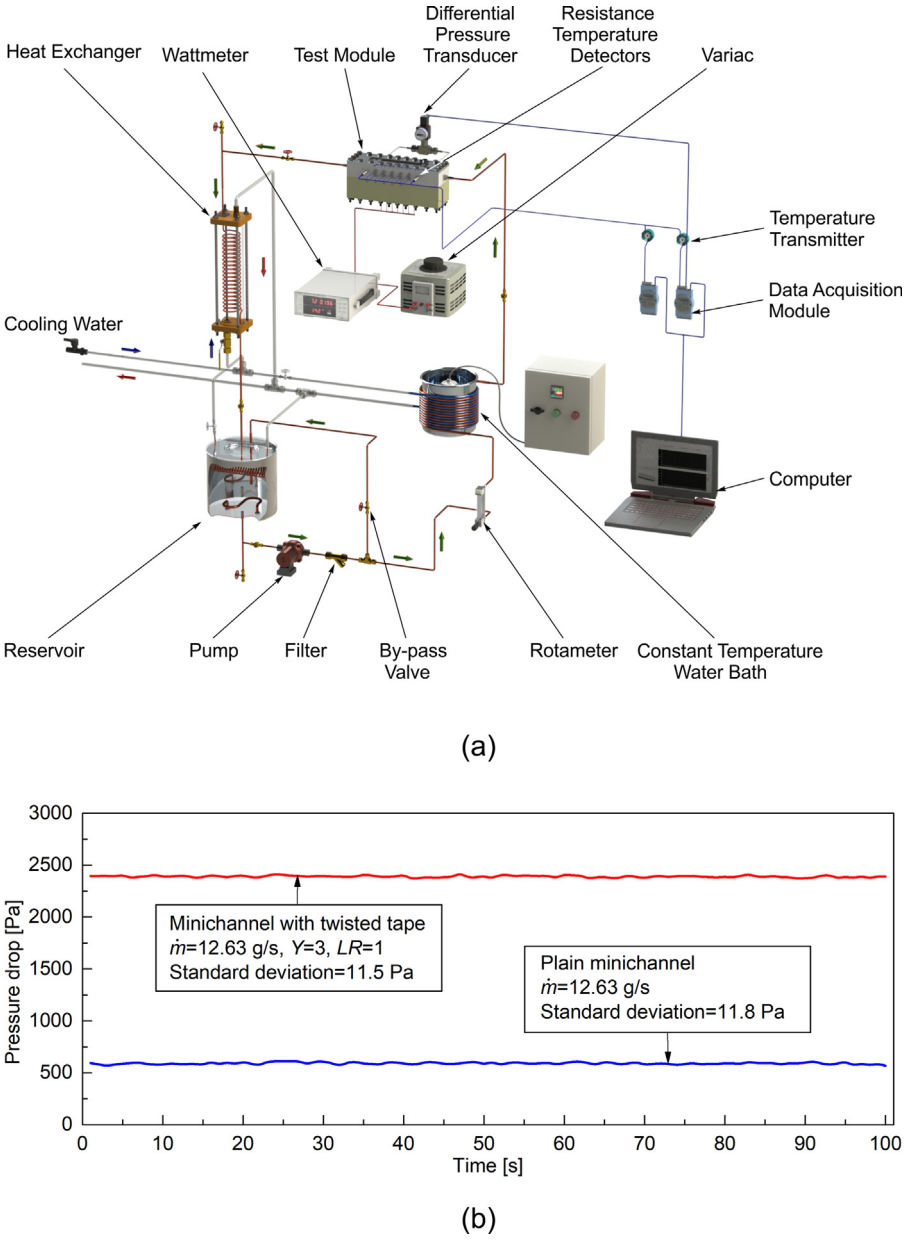

Fig. 2. (a) Schematic diagram of experimental flow loop. (b) Pressure drop fluctuation in the minichannels with and without twisted tape.

Table 1
Accuracy of measuring instruments.

Property	Instrument	Accuracy
Dimension	Vernier caliper	0.02 mm
Temperature	RTD Pt100	0.1 °C
Pressure drop	Star Meter, CCY 150	0.25% of full scale
Volumetric flow rate	Shuanghuan, LZB-6WB	2.5% of full scale
Heater Power	EVERFINE, PF9800	0.5% of full scale

3. Data reduction and uncertainty analysis

3.1. Data reduction

The mass flow rate, $\dot{m}$, is expressed as Eq. (1).

$$\dot{m} = \dot{V}\rho_{in} \tag{1}$$

where $\dot{V}$ is the volumetric flow rate; ρ_{in} is the density of the fluid at the test module's inlet.

The inlet velocity of single plain minichannel, u_{in}, is given by Eq. (2).

$$u_{in} = \frac{\dot{V}}{N_{ch}W_{ch}H_{ch}} \tag{2}$$

where N_{ch} is the total number of minichannels, N_{ch}=8; W_{ch} and H_{ch} are the width and height of single minichannel, respectively, W_{ch}=H_{ch}=2 mm.

The Reynolds number for single plain minichannel, Re_0, is defined as Eq. (3) based on inlet parameters.

$$Re_0 = \frac{\rho_{in}u_{in}D_h}{\mu_{in}} \tag{3}$$

where μ_{in} is the dynamic viscosity of the fluid at the test module's inlet; D_h is the hydraulic diameter of the plain minichannel, D_h=$2W_{ch}H_{ch}/(W_{ch}+H_{ch})$.

Because the total pressure drop, ΔP_{tot}, measured by differential pressure transducer, includes the pressure drops along the minichannels and the plenums at inlet and outlet, as well as the

pressure losses due to the abrupt contraction and expansion, the pressure drop between the inlet and outlet of minichannel, ΔP_{ch}, is calculated by Eq. (4).

$$\Delta P_{ch} = \Delta P_{tot} - \left(\Delta P_c + \Delta P_{ip} + \Delta P_{op} + \Delta P_e\right) \tag{4}$$

where ΔP_c and ΔP_e are the inlet contraction and outlet expansion pressure losses, respectively. They are expressed as Eq. (5) and Eq. (6), respectively.

$$\Delta P_c = 0.25\left\{\left[1-\left(\frac{A_{isp}}{A_{idp}}\right)^2\right]\rho_{in}u_{isp}^2 + \left[1-\left(\frac{A_{chs}}{A_{isp}}\right)^2\right]\rho_{in}u_{in}^2\right\} \tag{5}$$

$$\Delta P_e = 0.5\left[\left(1-\frac{A_{chs}}{A_{osp}}\right)^2\rho_{out}u_{out}^2 + \left(1-\frac{A_{osp}}{A_{odp}}\right)^2\rho_{out}u_{osp}^2\right] \tag{6}$$

where A_{chs}, A_{isp}, A_{idp}, A_{osp} and A_{odp} are the cross-sectional areas of the total minichannels, inlet shallow plenum, inlet deep plenum, outlet shallow plenum and outlet deep plenum, respectively; u_{out}, u_{isp} and u_{osp} are the velocities at the minichannel outlet, inlet shallow plenum and outlet shallow plenum, respectively; ρ_{out} is the dynamic viscosity of the fluid at the test module's outlet.

In Eq. (4), ΔP_{ip} and ΔP_{op} are the pressure drops across the inlet and outlet plenums, respectively. The pressure drops across the deep plenums can be ignored due to very low fluid velocities in the deep plenums, so ΔP_{ip} and ΔP_{op} only account for the shallow plenums. The inlet and outlet shallow plenums have same dimensions, thus ΔP_{ip} and ΔP_{op} are estimated from Eq. (7) and Eq. (8), respectively.

$$\Delta P_{ip} = \frac{2f_{isp}u_{isp}^2L_{sp}\rho_{in}}{D_{h,sp}} \tag{7}$$

$$\Delta P_{op} = \frac{2f_{osp}u_{osp}^2L_{sp}\rho_{out}}{D_{h,sp}} \tag{8}$$

where L_{sp} and $D_{h,sp}$ are the length and hydraulic diameter of the shallow plenum, respectively; f_{isp} and f_{osp} are the Fanning friction factors in inlet and outlet shallow plenums, respectively, which are obtained from Eq. (9) [37].

$$f_kRe_k = 24\left(1-1.3553\alpha+1.9467\alpha^2-1.7012\alpha^3+0.9564\alpha^4-0.2537\alpha^5\right) \tag{9}$$

where subscript k refers to either inlet shallow plenum, *isp*, or outlet shallow plenum, *osp;* α is aspect ratio of rectangular channel; Re_k is the Reynolds number and defined as Eq. (10).

$$Re_k = \frac{\rho_k u_k D_{h,sp}}{\mu_k} \tag{10}$$

The pressure drop per unit length in the minichannel, ΔP_{pul}, is defined as Eq. (11).

$$\Delta P_{pul} = \frac{\Delta P_{ch}}{L_{ch}} \tag{11}$$

where L_{ch} denotes the length of the minichannel, L_{ch}=150 mm.

The heat input to the fluid across the minichannels, $\dot{Q}$, is evaluated from Eq. (12) using an energy balance.

$$\dot{Q} = \dot{V}\rho_{in}c_{p,m}(T_{out}-T_{in}) \tag{12}$$

where $c_{p,m}$ is the fluid specific heat at constant pressure based on the average fluid bulk temperature; T_{in} and T_{out} are the inlet and outlet temperatures, respectively. Furthermore, the base heat flux, q, is expressed as Eq. (13).

$$q = \frac{\dot{Q}}{A_t} \tag{13}$$

where A_t is the footprint area of the heat sink top platform, $A_t = 25\times150$ mm^2.

The temperature of the minichannel's bottom wall is not equal to the temperature measured by RTD due to the thermal resistance of copper. Therefore, the Fourier's law of heat conduction is used to determine this temperature. Assuming one-dimensional heat conduction between the minichannel's bottom wall and the plane of the RTDs, the local temperature of the minichannel's bottom wall, $T_{w,n}$, can be calculated by Eq. (14).

$$T_{w,n} = T_{R,n} - \frac{qH_R}{k_s} \tag{14}$$

where subscript n denotes the location number of RTD; $T_{R,n}$ is the temperature measured by the number n RTD (see Fig. 1(a)); H_R denotes the distance from the center of RTD junction to the minichannel's bottom wall, H_R=5 mm; k_s represents the thermal conductivity of the heat sink, k_s=398 W/m K. Furthermore, the average temperature of the minichannel's bottom wall, $T_{w,ave}$, can be obtained by Eq. (15).

$$T_{w,ave} = \frac{1}{5}\sum_{n=1}^{5}T_{w,n} \tag{15}$$

Because the intermediate walls between the minichannels act as fins, the average heat transfer coefficient, h_{ave}, can be determined using an energy balance with the fin analysis method, as follows:

$$h_{ave} = \frac{qW_s}{N_{ch}(W_{ch}+2\eta_{fin}H_{ch})[T_{w,ave}-T_{f,ave}]} \tag{16}$$

where W_s is the width of the heat sink top platform, W_s=25 mm; $T_{f,ave}$ is the average bulk fluid temperature, $T_{f,ave}=(T_{in}+T_{out})/2$; η_{fin} is the fin efficiency. The fin tips are assumed to be adiabatic because the insulating Pyrex glass is employed for the cover plate. For a rectangular fin with an adiabatic tip, η_{fin} is defined as Eq. (17).

$$\eta_{fin} = \frac{\tanh(mH_{ch})}{mH_{ch}} \tag{17}$$

where m is the fin parameter and given by Eq. (18).

$$m = \sqrt{\frac{2(L_{ch}+W_{fin})h_{ave}}{k_sL_{ch}W_{fin}}} \tag{18}$$

in which W_{fin} is the width of the fin between two adjacent minichannels, W_{fin}=1 mm. Solving Eqs. (16)–(18) with an iterative scheme yields the average heat transfer coefficient, h_{ave}.

For evaluating the comprehensive effects of the twisted tapes on the fluid flow and heat transfer performances in the minichannels, a thermal enhancement factor, η, is introduced in present work. The thermal enhancement factor is defined as the ratio of the average heat transfer coefficient in the minichannels with twisted tapes, h_{ave}, to that without twisted tapes, $h_{ave,0}$, at the same pumping power. This factor is given by Eq. (19).

$$\eta = \left.\frac{h_{ave}}{h_{ave,0}}\right|_{PP} = \frac{h_{ave}/h_{ave,0}}{\left(\Delta P_{pul}/\Delta P_{pul,0}\right)^{1/3}} \tag{19}$$

where $\Delta P_{pul,0}$, represents the pressure drop per unit length in the minichannels without twisted tapes (i.e. plain minichannels).

3.2. Uncertainty analysis

Uncertainty analysis in present work is performed using method proposed by Moffat [38]. The accuracy of measuring instruments employed in present experiment is listed in Table 1. The uncertainty for measuring instrument with accuracy at full scale can be calculated by $\delta p = R_{ins}A_{ins}/\sqrt{3}$; where δp is the uncertainty

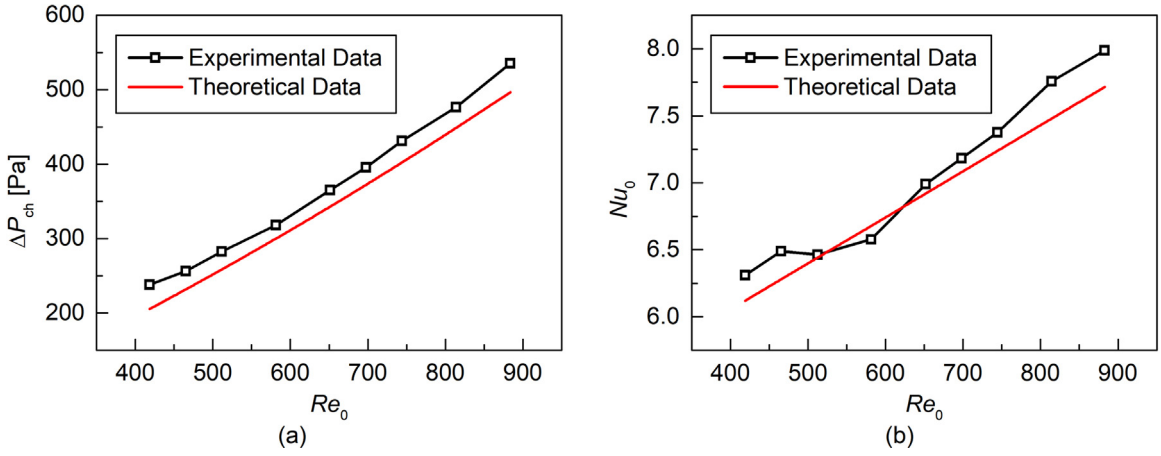

Fig. 3. Comparisons of experimental data with theoretical data for (a) pressure drop, and (b) Nusselt number in the plain minichannels.

in measuring parameter, p; R_{ins} and A_{ins} are the range and accuracy of instrument, respectively. The relative uncertainty (as a percentage) of the derived quantities can be calculated from Eq. (20).

$$\frac{\delta R}{R} = \frac{1}{R}\left[\sum_{i=1}^{N}\left(\frac{\partial R}{\partial X_i}\delta X_i\right)^2\right]^{1/2} \tag{20}$$

where δR, δX_i are the uncertainties of the derived quantity, R, and the measured parameter, X_i, respectively. According to Eq. (20), the uncertainties of Reynolds number in the plain minichannel, pressure drop per unit length and heat transfer coefficient can be estimated to be in the ranges of 2.33–3.94%, 1.21–11.39% and 3.45–4.18%, respectively, in the present study. More details about the uncertainties are given in Appendix A.

4. Results and discussion

4.1. Validation of experimental methods

In order to validate the reliabilities of experimental setup and data reduction methods, the experimental data of pressure drop and Nusselt number in the plain minichannel are compared with theoretical data, which are calculated by Eqs. (21)–(27).

For the developing laminar flow region in the rectangular channel, Steinke and Kandlikar [37] provided the expression of theoretical pressure drop, which is given by Eq. (21).

$$\Delta P = \frac{2Po\mu_m u_m L_{ch}}{D_h^2} + \frac{K(\infty)\rho_m u_m^2}{2} \tag{21}$$

where Po is the Poiseuille number, Po=fRe, calculated by Eq. (9); μ_m is the dynamic viscosity based on the average fluid bulk temperature; u_m is the average velocity; $K(\infty)$ is the Hagenbach's factor, given by Eq. (22) [37].

$$K(\infty) = 0.6797 + 1.2197\alpha + 3.3089\alpha^2 - 9.5921\alpha^3 + 8.9089\alpha^4 - 2.9959\alpha^5 \tag{22}$$

For the thermally developing laminar flow region, the local Nusselt number, Nu_x, is determined according to Shah and London's correlation [39], as follows:

$$Nu_x = 4.363 + 8.68\left(10^3 x^*\right)^{-0.506}\exp(-41x^*) \tag{23}$$

$$x^* = \frac{x}{RePrD_h},\quad Pr = \frac{c_{p,x}\mu_x}{k_{f,x}} \tag{24}$$

where x is the distance to the minichannel inlet; x^* is the dimensionless axial distance; Pr is the Prandtl number. Because the minichannel in present work is the three-sided heating configuration, the following relation is adopted to predict the local Nusselt number for present work [40]:

$$Nu_{x,3} = \left(\frac{Nu_3}{Nu_4}\right)Nu_x \tag{25}$$

where $Nu_{x,3}$ refers to the local Nusselt number for the thermally developing region with three-sided heating; Nu_3 and Nu_4 are the Nusselt numbers in the thermally developed region for the three-sided and four-sided heating cases, respectively. They are given by Eq. (26) and Eq. (27) [39], respectively.

$$Nu_3 = 8.235\left(1 - 1.883\alpha + 3.767\alpha^2 - 5.814\alpha^3 + 5.361\alpha^4 - 2.0\alpha^5\right) \tag{26}$$

$$Nu_4 = 8.235\left(1 - 2.042\alpha + 3.085\alpha^2 - 2.477\alpha^3 + 1.058\alpha^4 - 0.186\alpha^5\right) \tag{27}$$

In the present experiment, the Nusselt number for plain minichannel, Nu_0, is calculated by Eq. (28).

$$Nu_0 = \frac{h_{ave,0}D_h}{k_{f,m}} \tag{28}$$

where $k_{f,m}$ is the fluid thermal conductivity based on the average fluid bulk temperature.

Fig. 3 compares the experimental data with the theoretical data for both pressure drop (q=0 W/m^2), and Nusselt number in the plain minichannels, which presents a reasonably good agreement. The maximum and mean absolute deviations for pressure drop are 16.0% and 8.5%, respectively, and for Nusselt number are 3.7% and 2.2%, respectively. This suggests that the experimental setup and data reduction methods adopted in present work are reliable for the investigation on the hydraulic and thermal performances. Additionally, it is found from Fig. 3(b) that the Nusselt number increases with Reynolds number increasing except one data point at Re_0= 512. This phenomenon is also found in Ref. [41]. This is possibly because of experimental error. Furthermore, comparing Nu_0 at Re_0= 512 with Nu_0 at Re_0= 465 and Nu_0 at Re_0= 581, it is found that their deviations are very small (<1.74%).

4.2. Effects of twisted tapes on flow and heat transfer performances

4.2.1. Effect of twist ratio

Fig. 4 shows variation of the pressure drop per unit length, ΔP_{pul}, with the twist ratio of twisted tape, Y, for different tape-length ratios and mass flow rates. For a given tape-length ratio and the same mass flow rate, the pressure drop per unit length generally decreases with increasing twist ratio, i.e., the pressure drop

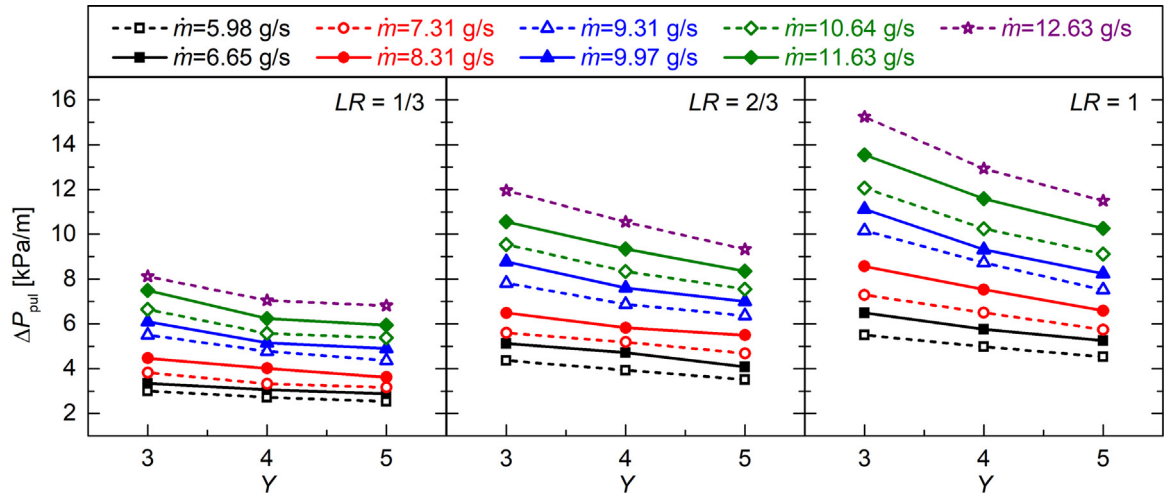

Fig. 4. Variation of pressure drop per unit length with the twist ratio of twisted tape for different tape-length ratios and mass flow rates.

per unit length increases with the decrease in twist ratio. For instance, at the tape-length ratio of 2/3 and mass flow rate of 5.98 g/s (Re_0=419), the pressure drop per unit length for twist ratios of 3 and 4 are increased by 24.3% and 11.9%, respectively, as compared to the twist ratio of 5. This is attributed to the existence of swirl flow and the increase in flow path. The previous studies [16-19] proved that the swirls were generated into the fluid passing the twisted tape. It is well known that the swirl will bring pressure loss. The stronger swirl intensity is generated by the smaller twist ratio of twisted tape, thereby causing the greater pressure loss. Moreover, the addition of twisted tape in the plain minichannel renders the straight flow to become the swirl flow. This type of flow results in the flow path increasing for the same distance in the axial direction, meaning the flow resistance increasing. Thus, smaller twist ratio results in longer flow path and larger pressure loss. Furthermore, with reducing twisted ratio of twisted tape, the increase in frictional area is one of reasons for increasing pressure loss. As the same length, same width and same thickness of the twisted tape, reducing the twist ratio causes the surface of twisted tape to extend. This suggests that more fluid contact with walls of the twist tape, thereby increasing the flow resistance. In conclusion, decreasing twist ratio results in the flow resistance increasing, thereby raising the pressure drop per unit length.

Apparently, the swirl flow generated by twisted tape leads to redistribution of the fluid temperature field, thereby affecting the wall temperature distribution. Fig. 5(a) depicts the distribution of wall temperature along the plain minichannel and twisted tape inserted minichannels with different twist ratios (Y=3, 4, 5) at given tape-length ratios (LR=1/3, 2/3, 1) and mass flow rate of 11.63 g/s (Re_0=814). It is clearly seen that, the wall temperatures for twisted tape inserted minichannels are much lower than that for the plain minichannel at a given location x. For example, at the tape-length ratio LR=2/3 and axial location x=75 mm, the wall temperatures for twisted tape inserted minichannels with twist ratios of 3, 4 and 5 are 7.7, 7.0 and 6.6 K lower than that for the plain minichannel, respectively. This indicates that the presence of twisted tape can improve heat transfer performance in the minichannel. This behavior can be attributed to the swirl flow generated by twisted tapes, which can promote the mixing between cold and hot fluid, thereby disturbing the flow boundary layer and reducing the thickness of thermal boundary layer. Thus, the heat transfer performance is enhanced in the twisted tape inserted minichannel. Moreover, this enhanced effect closely correlates with the twist ratio of twisted tape. Smaller twist ratio results in better heat transfer enhancement. This is because smaller twist ratio induces stronger swirl flow intensity.

Fig. 5(b) illustrates variation of the average heat transfer coefficient, h_{ave}, with twist ratio of the twisted tape, Y, for different tape-length ratios and mass flow rates. The trends of average heat transfer coefficient with twist ratio are similar to that of pressure drop per unit length, i.e., the average heat transfer coefficient increases with the decrease in twist ratio. For instance, at the tape-length ratio of 1 and mass flow rate of 8.31 g/s (Re_0=581), the average heat transfer coefficients for twist ratios of 3 and 4 are increased by 24.4% and 8.2%, respectively, as compared to the twist ratio of 5. As discussed earlier, smaller twist ratio can induce stronger swirl flow, thereby enhancing the disturbance of the fluid and flow boundary layer. It is helpful to mix the hot and cold fluid, and reduce the thickness of boundary layer. Furthermore, the decrease in twist ratio can promote the length of fluid flow path, rendering the mixing time of the hot and cold fluid to increase. As a consequence, the heat transfer enhancement is achieved by decreasing the twist ratio of twisted tape.

4.2.2. Effect of tape-length ratio

Fig. 6 presents the variation of pressure drop per unit length, ΔP_{pul}, with tape-length ratio, LR, for different twist ratios (Y=3, 4, 5) and mass flow rates. It can be obviously observed that the pressure drop per unit length increases with the tape-length ratio increasing at a given twist ratio and the same mass flow rate. For instance, at the twist ratio of 3 and mass flow rate of 9.97 g/s (Re_0=698), the minichannels with tape-length ratios of 2/3 and 1 respectively yield 43.8% and 82.1% greater pressure drops per unit length as compared to the minichannel with tape-length ratio of 1/3. This is because longer twisted tape produces wider coverage of swirl flow, greater frictional surface area and longer fluid flow path, thereby bringing greater form resistance and frictional resistance.

Fig. 7(a) shows the distribution of wall temperature along the plain minichannel and twisted tape inserted minichannels with different tape-length ratios (LR=1/3, 2/3, 1) at given twist ratios (Y=3, 4, 5) and mass flow rate of 11.63 g/s (Re_0=814). It is clear that the wall temperature escalates along the minichannel. For the plain minichannel, the wall temperature increases speedily in the upstream of the minichannel, but slowly in the downstream. This trend is consistent with the experimental and numerical results of Qu and Mudawar [42]. This is due to the fact that, on the one hand, the thermal and hydrodynamic boundary layers are devel-

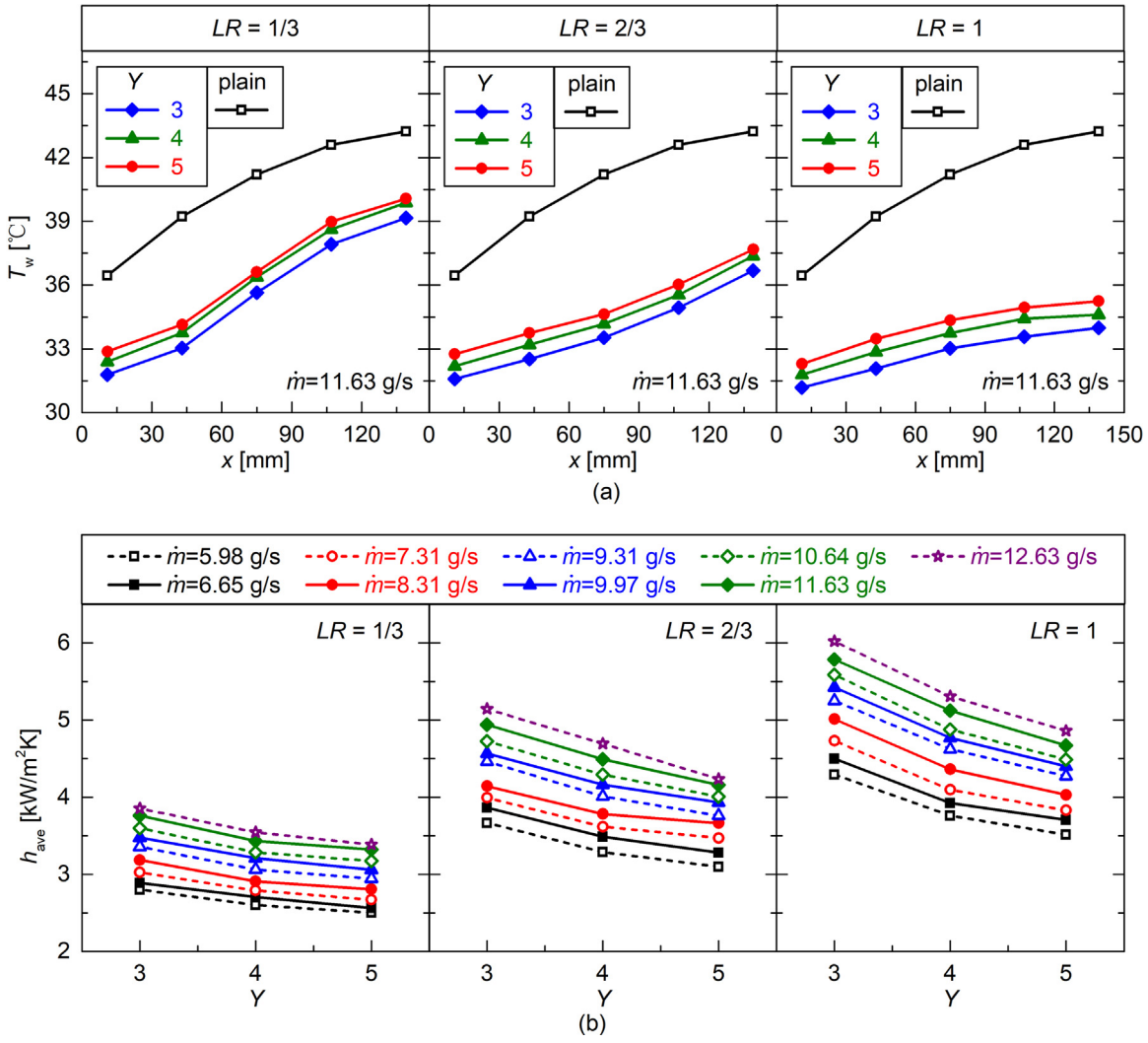

Fig. 5. (a) Distribution of wall temperature along the plain minichannel and twisted tape inserted minichannels with different twist ratios at given tape-length ratios and $\dot{m}$=11.63 g/s. (b) Variation of average heat transfer coefficient with twist ratio of the twisted tape for different tape-length ratios and mass flow rates.

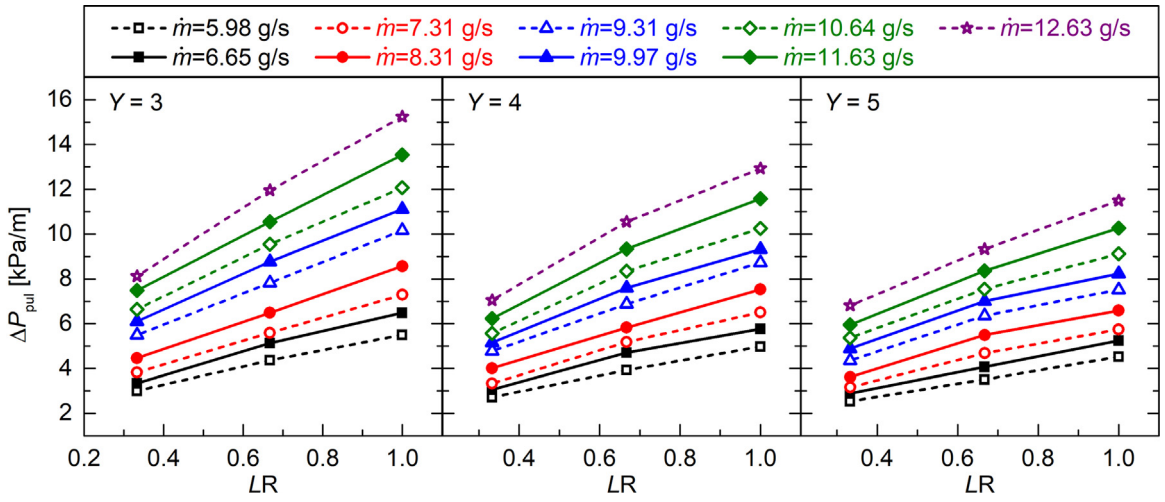

Fig. 6. Variation of pressure drop per unit length with the tape-length ratio for different twist ratios and mass flow rates.

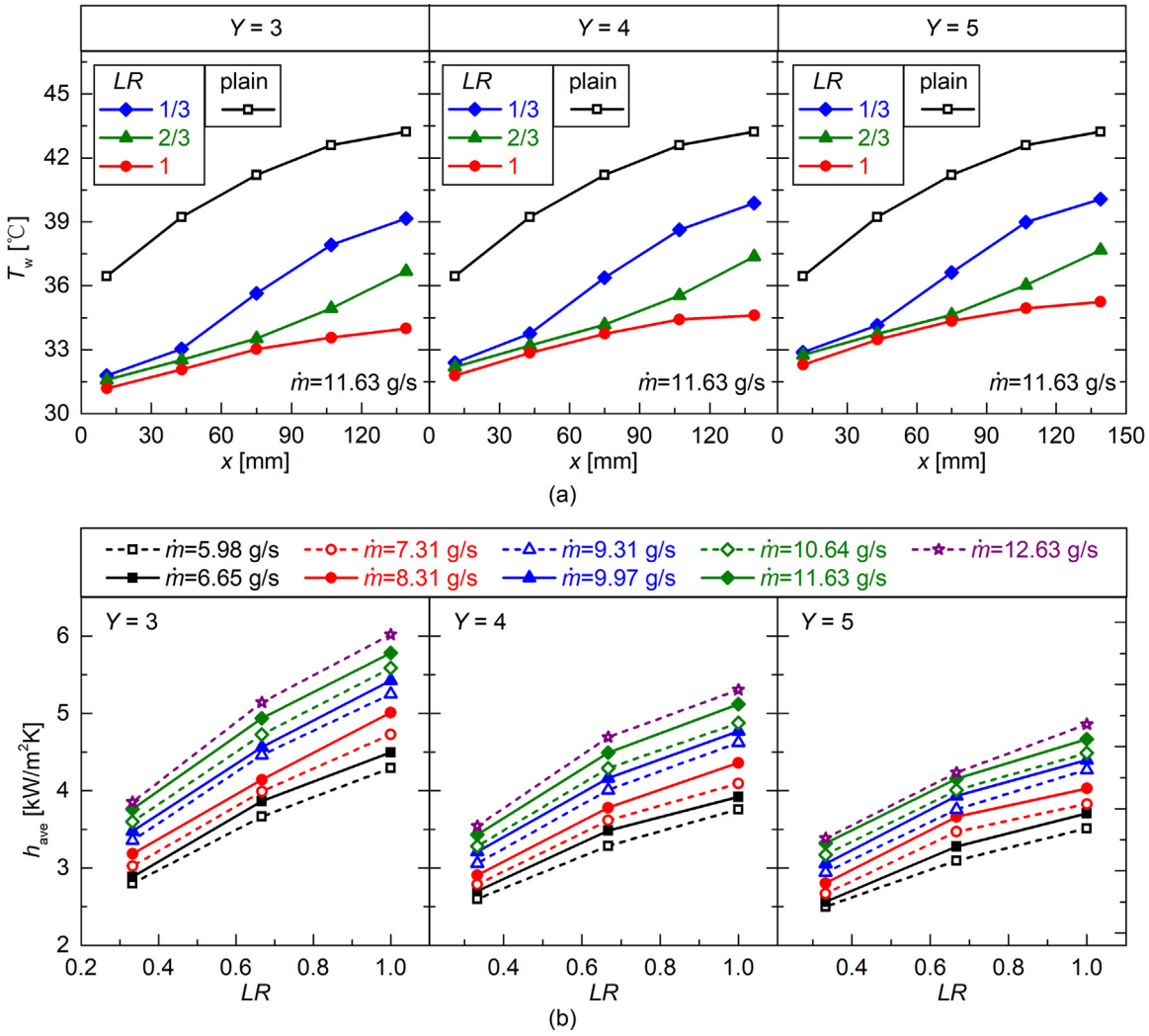

Fig. 7. (a) Distribution of wall temperature along the plain minichannel and twisted tape inserted minichannels with different tape-length ratios at given twist ratios and $\dot{m}$=11.63 g/s. (b) Variation of average heat transfer coefficient with tape-length ratio for different twist ratios and mass flow rates.

oping in the upstream, resulting in the existence of an entrance effect; but the boundary layer trends toward fully developed state in the downstream, rendering thermal resistance to escalate. On the other hand, the temperature of working fluid in the upstream is low, thereby promoting heat transfer; but in the downstream, the temperature of working fluid is high because the heat has injected into fluid from heating wall where the fluid flows through. It is not beneficial to heat transfer between the heating wall and fluid. For all minichannels with twisted tape, the wall temperatures along the flow direction escalate mildly in the upstream; but in the midstream and downstream, the trends of wall temperature are different due to different tape-length ratios. Taking the instance of minichannel with the tape-length ratio of 1/3 (L_t=50 mm), the wall temperature along minichannel increases speedily in the midstream, while slowly in the downstream. This trend is similar to that of plain minichannel. This is because of both midstream and downstream regions without twisted tape, indicating no swirl flow existing or weak swirl flow intensity. It is interesting to find that for the minichannel with tape-length ratio of 1 (i.e., full-length twisted tape, L_t=150 mm), the wall temperature escalates slightly along whole channel. In addition, the temperature difference between maximum and minimum wall temperature is lower as compared to the plain minichannel and other twisted tape inserted minichannels. For instance, at twist ratio of 3, the wall temperature difference for tape-length ratio of 1 is 2.8 K, while that for tape-length ratios of 1/3 and 2/3 are 7.6 and 5.1 K, respectively, and that for plain minichannel is 6.8 K. This suggests that the minichannel with full-length twisted tape has the best uniformity of wall temperature distribution on the heat sink base. However, the minichannel with shorter twisted tape (LR=1/3) has worst uniformity of wall temperature distribution. This is because of the entrance effect and stronger swirl flow in the upstream as compared to midstream and downstream. This issue is able to be solved by placing the twisted tape in the midstream or downstream of minichannel. In general, the region having twisted tape in the minichannel can reduce wall temperature as compared to the region without twisted tape, indicating enhancement of heat transfer performance. Longer twisted tape yields lower average wall temperature. For a given twist ratio, the minichannel with full-length twisted tape produces the lowest wall temperature and the best uniformity of wall temperature distribution.

Fig. 7(b) shows the variation of the average heat transfer coefficient, h_{ave}, with different tape-length ratios (LR=1/3, 2/3, 1) in the twisted tape inserted minichannels for different mass flow rates at given twist ratios (Y=3, 4, 5). As expected, the average heat transfer coefficient increases with the increase in the tape-length ratio

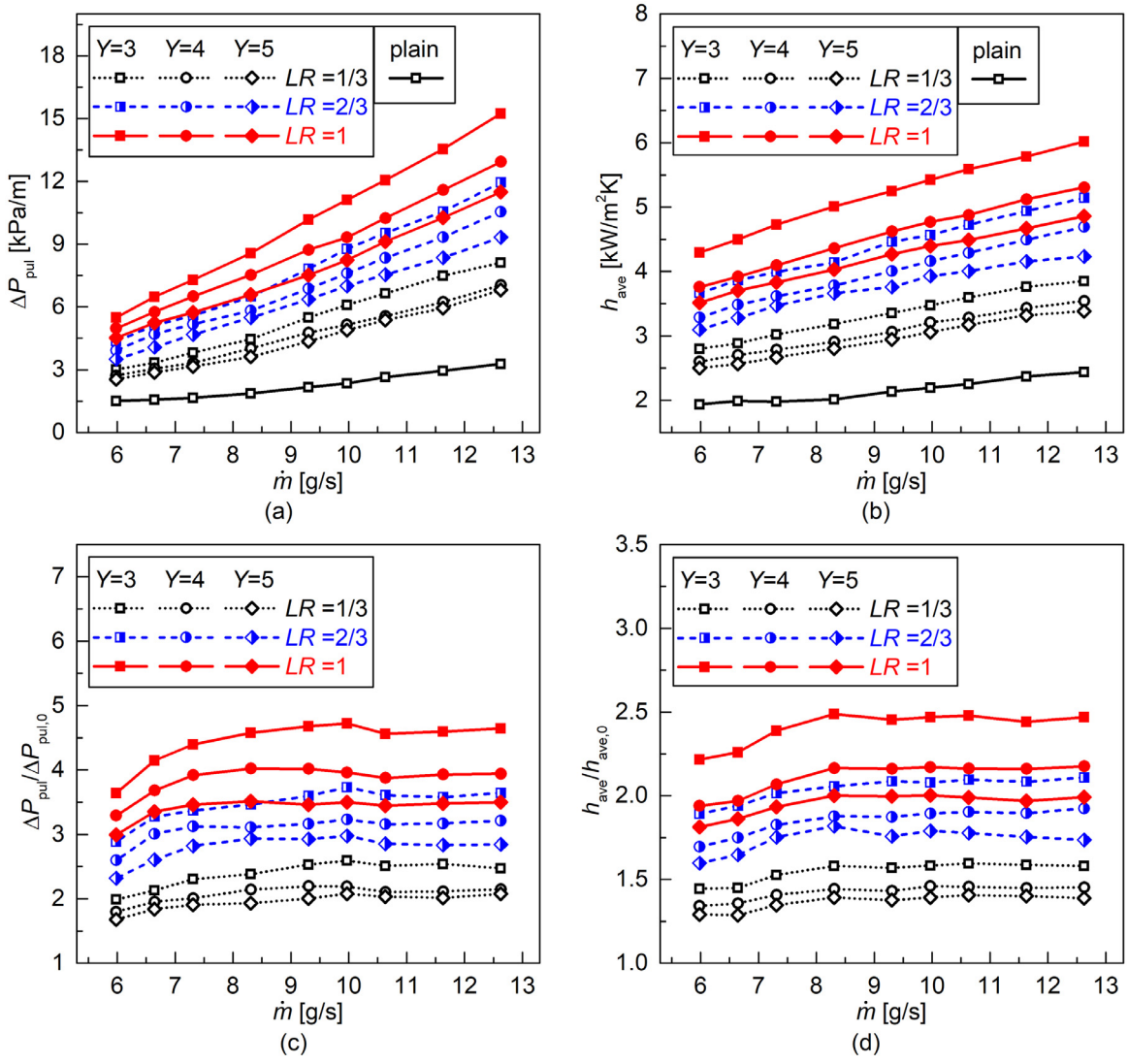

Fig. 8. Variations of (a) pressure drop per unit length, (b) average heat transfer coefficient, (c) $\Delta P_{pul}/\Delta P_{pul,0}$ and (d) $h_{ave}/h_{ave,0}$ with mass flow rate.

at the given twist ratio and mass flow rate. For example, at the twist ratio of 3 and mass flow rate of 9.97 g/s (Re_0=698), the average heat transfer coefficients in the minichannels with tape-length ratios of 2/3 and 1 are increased by 31.3% and 56.0%, respectively, as compared to that with tape-length ratio of 1/3. This is because for the minichannel with shortest twisted tape (LR=1/3) placed in the upstream, the swirling flow are generated in the upstream as the fluid passing the twisted tape. As earlier discussed, this type of flow can enhance heat transfer performance in the upstream. However, with the fluid passing through the downstream without twisted tape, the swirling flow becomes weak, even changes to the straight flow. According to the field synergy theory proposed by Guo et al. [43], such type of flow isn't helpful to the improvement of the convective heat transfer. With the tape-length ratio increasing, e.g. full-length twisted tape (LR=1), the swirling flow fully fills in the whole minichannel, meaning heat transfer enhancement for the whole minichannel. In general, the minichannels with full-length twisted tape (LR=1) show the best heat transfer performance. The maximum average heat transfer coefficient reaches 6.02 kW/m^2 K at the twist ratio of 3 and mass flow rate of 12.63 g/s (Re_0=884).

4.3. Effects of mass flow rate on flow and heat transfer performances

Fig. 8(a) and (b) presents the variations of pressure drop per unit length and average heat transfer coefficient with mass flow rate. As shown in Fig. 8(a), the pressure drop per unit length increases with the increase in mass flow rate for all cases. Especially for the cases with full-length twisted tape (LR=1), their increased rates are greater than that of plain minichannel. This is because with mass flow rate increasing, the fluid velocity gradient increases, resulting in the enhancements of shear stresses between fluid and fluid as well as between fluid and wall, and the enhancement of swirl intensity in the twisted tape inserted minichannel, thereby increasing pressure loss. Apparently, the full-length twisted tape brings more pressure loss. From Fig. 8(b), it is clearly seen that the heat transfer coefficient increases with the mass flow rate increasing regardless of minichannel with or without twisted tape. Also, the increased rate for the twisted tape inserted minichannel is substantially larger than that for plain minichannel, especially for the twisted tape inserted minichannel with Y=3 and LR=1. This can be explained by the fact that increasing mass flow rate can improve the velocity gradient near the minichannel wall,

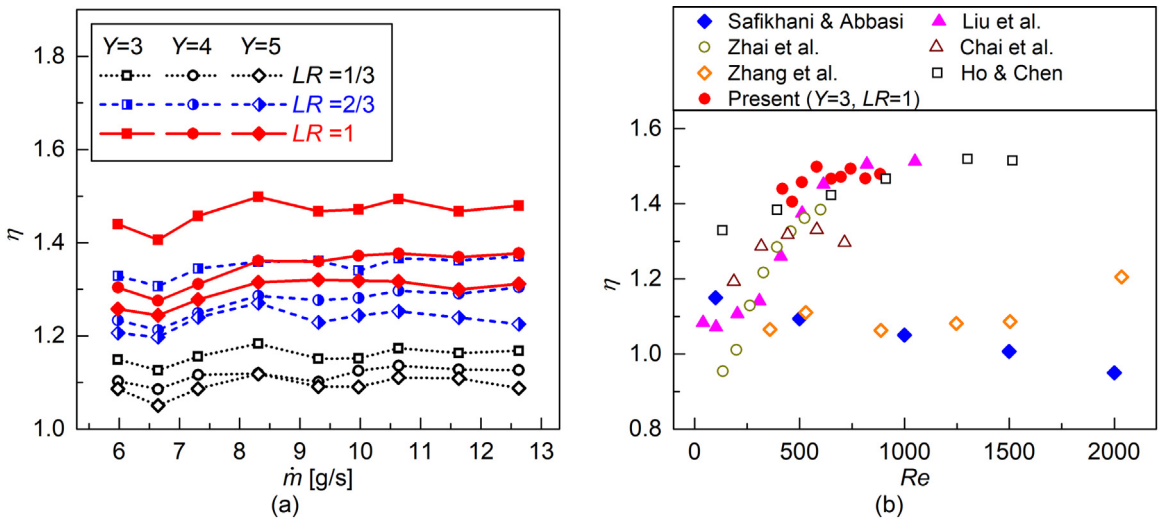

Fig. 9. (a) Variation of thermal enhancement factor with mass flow rate. (b) Overall thermal performance comparison with the previous studies: Safikhani and Abbasi [44], Liu et al. [19], Zhai et al. [45], Chai et al. [46], Zhang et al. [47], and Ho and Chen [48].

thereby thinning thermal boundary layer. For the twisted tape inserted minichannel, the increase of mass flow rate also enhances the swirl intensity, further facilitating fluid mixing and disturbing thermal boundary layer, thereby leading to better heat transfer enhancement. Obviously, the effect of enhancement is more remarkable for twisted tape with smaller twist ratio or/and longer length.

Fig. 8(c) and (d) gives the variations of the pressure drop increasing factor ($\Delta P_{pul}/\Delta P_{pul,0}$) and heat transfer enhancement factor ($h_{ave}/h_{ave,0}$) with mass flow rate, where $\Delta P_{pul,0}$ and $h_{ave,0}$ denote the pressure drop per unit length and average heat transfer coefficient in the plain minichannel, respectively. From Fig. 8(c) and (d), it is found that with mass flow rate increasing, both $\Delta P_{pul}/\Delta P_{pul,0}$ and $h_{ave}/h_{ave,0}$ rise slightly at the low mass flow rate and have no distinct change at the high mass flow rate, especially for full-length twisted tapes. This may be explained by the fact that at the low mass flow rate, the intensity of swirl flow caused by twisted tape is weak, resulting in low flow resistance and heat transfer augment. With the mass flow rate increasing, disturbing effect caused by twisted tape becomes strong, rendering effects of flow resistance and heat transfer augment to increase. However, this augment effect will reach a limit at the high mass flow rate as compared to plain minichannel because high velocity also results in strong disturbing effect for plain minichannel. In general, at the whole range of mass flow rate, the values of $\Delta P_{pul}/\Delta P_{pul,0}$ in twisted tape inserted minichannels with Y=3 and LR=1/3, Y=3 and LR=2/3, Y=3 and LR=1, Y=4 and LR=1/3, Y=4 and LR=2/3, Y=4 and LR=1, Y=5 and LR=1/3, Y=5 and LR=2/3, and Y=5 and LR=1 are in ranges of 1.99–2.59, 2.89–3.73, 3.64–4.72, 1.80–2.20, 2.60–3.23, 3.29–4.02, 1.68–2.08, 2.32–2.98 and 3.00–3.52, respectively. The values of $h_{ave}/h_{ave,0}$ in these cases are in ranges of 1.45–1.60, 1.89–2.11, 2.22–2.49, 1.34–1.46, 1.70–1.92, 1.94–2.18, 1.29–1.41, 1.60–1.82 and 1.81–2.00, respectively. For the same mass flow rate, the twisted tape inserted minichannel with Y=3 and LR=1 yields maximum $\Delta P_{pul}/\Delta P_{pul,0}$ and $h_{ave}/h_{ave,0}$, while that with Y=5 and LR=1/3 yields minimum $\Delta P_{pul}/\Delta P_{pul,0}$ and $h_{ave}/h_{ave,0}$.

4.4. Overall thermal performance

Above analysis shows that decreasing the twist ratio or increasing the tape-length ratio not only enhances the heat transfer performance, but also increases pressure drop in the twisted tape inserted minichannels. Therefore, to evaluate overall performance of flow and heat transfer in twisted tape inserted minichannels, a thermal enhancement factor (η) is introduced in present work and determined from Eq. (19). Fig. 9(a) presents the variation of thermal enhancement factor (η) with mass flow rate ($\dot{m}$) in different twisted tape inserted minichannels. From Fig. 9(a), it is clearly seen that the thermal enhancement factors for all the cases are greater than 1 at the whole range of mass flow rate, indicating that the heat transfer enhancement overwhelms the increase of pressure drop. This also suggests that the addition of the twisted tape can improve effectively the overall performance of the minichannel. It is observed that most of the variations in thermal enhancement factor mainly tend to be stable or have a slight uptrend as mass flow rate increasing. This is because the trend of heat transfer enhancement factor ($h_{ave}/h_{ave,0}$) with mass flow rate is similar to that of pressure drop increasing factor ($\Delta P_{pul}/\Delta P_{pul,0}$), as shown in Fig. 8(c) and (d). It is also observed that for a given mass flow rate, the thermal enhancement factor increases with the decrease in the twist ratio or/and the increase in the tape-length ratio, which is consistent with the trends of the heat transfer coefficient and pressure drop per unit length. This indicates that although twisted tape brings greater friction resistance with reducing the twist ratio or/and increasing the tape-length ratio, the heat transfer enhancement is much greater than the increase in friction resistance. Therefore, at the same mass flow rate the twisted tape inserted minichannel with Y=3 and LR=1 produces maximum value of thermal enhancement factor (maximum value is 1.50 at $\dot{m}$=8.31 g/s), and that with Y=5 and LR=1/3 yields minimum value (minimum value is 1.05 at $\dot{m}$=6.65 g/s). At the entire range of the study, the average values of thermal enhancement factor for twisted tape inserted minichannel with Y=3 and LR=1/3, Y=3 and LR=2/3, Y=3 and LR=1, Y=4 and LR=1/3, Y=4 and LR=2/3, Y=4 and LR=1, Y=5 and LR=1/3, Y=5 and LR=2/3, and Y=5 and LR=1 are 1.16, 1.35, 1.46, 1.12, 1.27, 1.35, 1.09, 1.23 and 1.30, respectively. Moreover, it is interesting to find that the average thermal enhancement factor (η=1.35) for twisted tape inserted minichannel with Y=3 and LR=2/3 is equal to that with Y=4 and LR=1. This is because both the decrease in the twisted ratio and the increase in the tape-length ratio can enhance the strength of the swirl and reduce its decay rate in the downstream of minichannel, thereby enhancing overall thermal performance. This enhancement effect for above two minichannels are almost same, i.e., when Y=4 and LR=2/3, the enhancement effect caused by decreasing twisted ratio (Y=3) is almost equivalent to that caused by increasing tape-length ratio (LR=1).

Table 2
Details of previous studies.

Authors	Geometry	Fluid	*Re*	Remarks
Safikhani and Abbasi [44]	Plain or flat tube with twisted tape D_h=10, 13.89 mm	Al_2O_3-water nanofluid	100–2000	η=0.95–1.15 for dual counter twisted tapes with Y=3
Liu et al. [19]	Tube with coaxial cross twisted tapes D_h=13 mm	Lubricating oil	40–1050	η=1.07–1.51 for coaxial cross twisted tapes with Y=4
Zhai et al. [45]	Rectangular microchannel with trapezoidal-cavity and circular-rib D_h=0.133 mm	Water	134–600	η=0.95–1.38 for relative cavity height of 0.3751 and relative rib height of 0.1365
Chai et al. [46]	Rectangular microchannel with fan-shaped ribs D_h=0.133 mm	Water	187–715	η=1.19–1.33 for H_r/W_c=0.25, H_r/W_c is the ratio of the height of rib to the width of microchannel
Zhang et al. [47]	Multiport minichannel flat tube D_h=1.65 mm	TiO_2-water nanofluid	359–2034	η=1.06–1.21 for nanofluid with average nanoparticle diameter of 10 nm and volume fraction of 0.01%
Ho and Chen [48]	Minichannel D_h=1.2 mm	Al_2O_3-water nanofluid	133–1515	η=1.33–1.52 for nanofluid with mass fraction of 10%

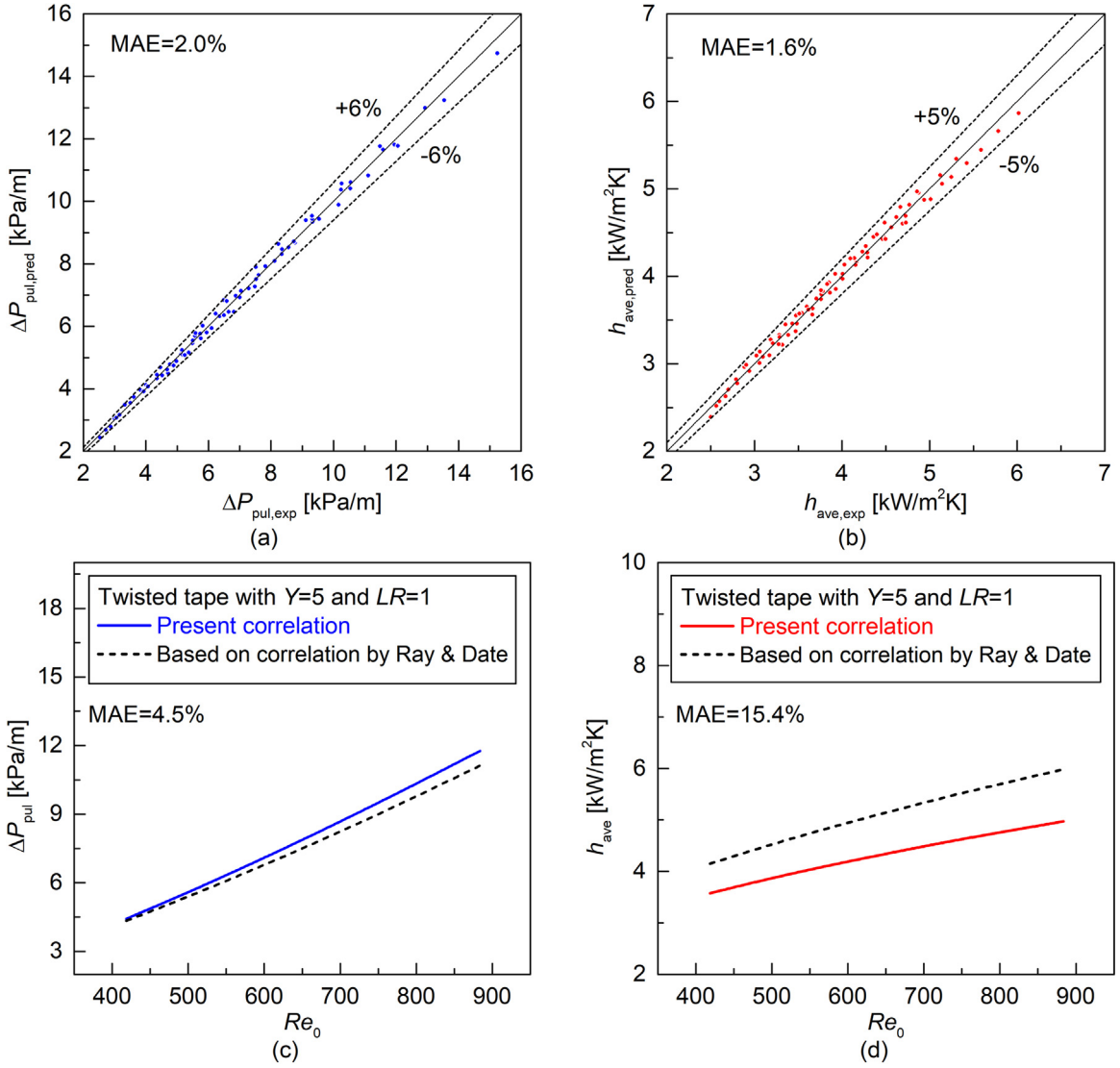

Fig. 10. Comparisons of predictions of present correlations with (a) experimental pressure drop per unit length, (b) experimental average heat transfer coefficient, (c) pressure drop per unit length based on correlation of Ray and Date [49], and (d) average heat transfer coefficient based on correlation of Ray and Date [49].

In addition, Fig. 9(b) presents the comparison of the best overall thermal performance obtained here (Y=3 and LR=1) with the previous studies: Safikhani and Abbasi [44], Liu et al. [19], Zhai et al. [45], Chai et al. [46], Zhang et al. [47], and Ho and Chen [48]. The details of the previous studies are shown in Table 2. It should be noted that the Reynolds number in Fig. 9(b) and Table 2 is based on plain channel parameters. The channels of top 2 studies in Table 2 are macro-scale channels, others are micro/mini-scale channels. From Fig. 9(b), it can be deduced that the thermal enhancement factor in the twisted tape inserted minichannel with Y=3 and LR=1 for present study is almost higher than that in other studies when Reynolds number is in range of 419–884. This means that the twisted tape inserted minichannel shows better overall thermal performance. Moreover, it has better practicability and reliability compared to Zhang et al. [47] and Ho and Chen [48] which working fluid are nanofluid. This is because nanofluid easily deposits during the system working.

4.5. Correlations for pressure drop per unit length and heat transfer coefficient

From the above analysis, it is expected that pressure drop per unit length or average heat transfer coefficient has great relationships with twist ratio (Y), tape-length ratio (LR) and mass flow rate. Also the Reynolds number in plain minichannel (Re_0) only depends on mass flow rate at given inlet temperature, and average heat transfer coefficient has great relationships with Prandtl number (Pr) as well [18]. In other words, pressure drop per unit length is correlated as a function of Y, LR and Re_0, while average heat transfer coefficient is correlated as a function of Y, LR, Re_0 and Pr. Therefore, based on 81 experimental data points in the minichannels with different twisted tapes, the empirical correlations for the pressure drop per unit length and average heat transfer coefficient have been developed using nonlinear regression analysis with aid of a data analysis software OriginPro. The two correlations were expressed as follows:

$$\Delta P_{\mathrm{pul}} = 3.3446 Y^{-0.4416} LR^{0.5458} Re_0^{1.3084} \tag{28}$$

$$h_{\mathrm{ave}} = 275.8204 Y^{-0.3251} LR^{0.3651} Re_0^{0.4167} Pr^{\frac{1}{3}} \tag{29}$$

where the physical property parameters in Pr are based on the arithmetic mean temperature of minichannel's inlet and outlet. The two correlations are suitable for $419 \le Re_0 \le 884$, $0.3333 \le LR \le 1$ and $5.4746 \le Pr \le 5.8442$. From Eqs. (28) and (29), the pressure drop per unit length and heat transfer coefficient increase with the decrease in twist ratio or/and the increase in tape-length ratio. With Reynolds number (mass flow rate) increasing, both pressure drop per unit length and heat transfer coefficient increase. This suggests that the trends obtained by Eqs. (28) and (29) agree well with the experimental trends. To further evaluate the reliability of developed empirical correlations, the predicted values of pressure drop per unit length and heat transfer coefficient correlations are compared with the experimental values, as shown in Fig. 10(a) and (b). It is found that the deviations between predicted values and experimental values for pressure drop per unit length are all within ±6% and that for heat transfer coefficient are all within ±5%. Moreover, the mean absolute errors (MAE) for pressure drop per unit length and heat transfer coefficient are 2.0% and 1.6%, respectively. This indicates excellent agreement between experimental and predicted values for both pressure drop per unit length and heat transfer coefficient. Furthermore, based on friction factor and Nusselt number correlations proposed by Ray and Date [49], the predicted values of pressure drop per unit length and heat transfer coefficient in the minichannel with full-length twisted tape can be calculated. Fig. 10(c) and (d) shows comparisons of predicted values of present correlations with that based on correlations proposed by Ray and Date [49] for twisted tape with Y=5 and LR=1. It is found that the trends of present correlations agree well with that based on correlations proposed by Ray and Date [49], as well as the MAE for pressure drop per unit length and heat transfer coefficient are 4.5% and 15.4%, respectively. This further verifies the effectiveness of present correlations.

5. Conclusions

The effects of twist ratio (Y=3, 4 and 5) and tape-length ratio (LR=1/3, 2/3 and 1) on the fluid flow and heat transfer performances in the square minichannel heat sink fitted with twisted tape inserts under laminar flow have been investigated experimentally. The following conclusions can be drawn from the present study:

1) Minichannel heat sink fitted with twisted tape inserts not only enhances the heat transfer performance, but also increases pressure drop, compared to the plain minichannel heat sink. Both average heat transfer coefficient (h_{ave}) and pressure drop per unit length (ΔP_{pul}) increase with the decrease in twist ratio or/and the increase in tape-length ratio. Thus, the twisted tape with Y=3 and LR=1 yields the best heat transfer performance and the highest pressure drop at the same mass flow rate. The heat transfer enhancement factor ($h_{\mathrm{ave}}/h_{\mathrm{ave,0}}$) and the pressure drop increasing factor ($\Delta P_{\mathrm{pul}}/\Delta P_{\mathrm{pul,0}}$) are in the ranges of 1.29–2.49 and 1.68–4.72, respectively.
2) The thermal enhancement factor (η) increases with the twist ratio reducing or/and the tape-length ratio increasing at the same mass flow rate. At the entire range of mass flow rate, the average values of η for each twisted tape are in a range of 1.09–1.46. The twisted tape with Y=3 and LR=1 yields the best overall thermal performance compared to other eight twisted tapes at the same mass flow rate. Thus, the twisted tape with Y=3 and LR=1 is more suitable for enhancing heat transfer in present study.
3) The empirical correlations for h_{ave} and ΔP_{pul} have been developed with relating to twist ratio (Y), tape-length ratio (LR), Reynolds number in plain minichannel (Re_0) or/and Prandtl number (Pr). The predicted h_{ave} and ΔP_{pul} calculated from those correlations are also fitted well with present experimental data, evidenced by standard deviations of ±5% and ±6%, respectively.

In future works, the following issue are worth investigating: (1) Although many numerical simulations on twisted tape were presented so far, the cases for twisted tape inside the rectangular channel were very few. Thus, to find the mechanism of heat transfer enhancement caused by twisted tape inside the rectangular micro/mini-channel, the simulation on flow and heat transfer characteristics in this heat sink needs to be investigated. (2) Two-phase micro/mini-channel heat sink achieves superior heat transfer rate by using both latent heat and sensible heat of coolant. However, the influences of twisted tape on heat transfer and flow performances in two-phase micro/mini-channel heat sink are not clear. Hence, this issue is worth investigating. (3) To evaluate the practical application value for the minichannel heat sink with twisted tape, it is necessary to establish the application of thermal management system integrated with the twisted tape inserted minichannel heat sink, and to conduct 3-E analysis [50] for this application in the future.

Declaration of Competing Interest

The authors declare that there is no conflict of interest.

CRediT authorship contribution statement

Zhenfei Feng: Conceptualization, Visualization, Funding acquisition, Methodology, Supervision, Project administration, Writing - original draft, Writing - review & editing. **Xin Ai:** Investigation, Methodology, Formal analysis, Visualization, Data curation, Validation, Writing - original draft. **Peilin Wu:** Software, Resources, Investigation, Validation. **Qingyu Lin:** Resources, Supervision. **Zuqiang Huang:** Funding acquisition, Supervision, Writing - review & editing.

Acknowledgments

The authors are grateful for the financial support from the National Natural Science Foundation of China (No. 21666005) and the Guangxi Natural Science Foundation of China (Nos. 2017GXNSFEA198001 and 2014GXNSFBA118051). This study is also supported by the Dean Project of Guangxi Key Laboratory of Petrochemical Resource Processing and Process Intensification Technology (No. 2019Z012) and the Scientific Research Foundation of Guangxi University (No. XBZ190875).

Appendix A

According to Eq. (20), the uncertainties of Reynolds number in the plain minichannel, pressure drop per unit length and heat transfer coefficient can be calculated from the following equations.

Reynolds number in the plain minichannel:

$$\frac{\delta Re_0}{Re_0} = \frac{1}{Re_0}\left[\left(\frac{\partial Re_0}{\partial u_{in}}\delta u_{in}\right)^2 + \left(\frac{\partial Re_0}{\partial D_h}\delta D_h\right)^2\right]^{1/2} = \left[\left(\frac{\delta u_{in}}{u_{in}}\right)^2 + \left(\frac{\delta D_h}{D_h}\right)^2\right]^{1/2} \tag{A1}$$

where $\delta u_{in}/u_{in}$ and $\delta D_h/D_h$ can be obtained from Eq. (A2) and Eq. (A3), respectively.

$$\frac{\delta u_{in}}{u_{in}} = \frac{1}{u_{in}}\left[\left(\frac{\partial u_{in}}{\partial \dot{V}}\delta \dot{V}\right)^2 + \left(\frac{\partial u_{in}}{\partial W_{ch}}\delta W_{ch}\right)^2 + \left(\frac{\partial u_{in}}{\partial H_{ch}}\delta H_{ch}\right)^2\right]^{\frac{1}{2}} = \left[\left(\frac{\delta \dot{V}}{\dot{V}}\right)^2 + \left(\frac{\delta W_{ch}}{W_{ch}}\right)^2 + \left(\frac{\delta H_{ch}}{H_{ch}}\right)^2\right]^{1/2} \tag{A2}$$

$$\frac{\delta D_h}{D_h} = \frac{1}{D_h}\left[\left(\frac{\partial D_h}{\partial W_{ch}}\delta W_{ch}\right)^2 + \left(\frac{\partial D_h}{\partial H_{ch}}\delta H_{ch}\right)^2\right]^{\frac{1}{2}} = \left[\left(\frac{\delta W_{ch}}{W_{ch}} - \frac{\delta W_{ch}}{W_{ch}+H_{ch}}\right)^2 + \left(\frac{\delta H_{ch}}{H_{ch}} - \frac{\delta H_{ch}}{W_{ch}+H_{ch}}\right)^2\right]^{1/2} \tag{A3}$$

Pressure drop per unit length:

$$\frac{\delta \Delta P_{pul}}{\Delta P_{pul}} = \frac{1}{\Delta P_{pul}}\left[\left(\frac{\partial \Delta P_{pul}}{\partial \Delta P_{ch}}\delta \Delta P_{ch}\right)^2 + \left(\frac{\partial \Delta P_{pul}}{\partial L_{ch}}\delta L_{ch}\right)^2\right]^{\frac{1}{2}} = \left[\left(\frac{\delta \Delta P_{ch}}{\Delta P_{ch}}\right)^2 + \left(\frac{\delta L_{ch}}{L_{ch}}\right)^2\right]^{1/2} \tag{A4}$$

where $\delta \Delta P_{ch}/\Delta P_{ch}$ is estimated to be $\delta \Delta P_{tot}/\Delta P_{tot}$.

Heat transfer coefficient:

$$\frac{\delta h_{ave}}{h_{ave}} = \frac{1}{h_{ave}}\left[\left(\frac{\partial h_{ave}}{\partial q}\delta q\right)^2 + \left(\frac{\partial h_{ave}}{\partial W_s}\delta W_s\right)^2 + \left(\frac{\partial h_{ave}}{\partial W_{ch}}\delta W_{ch}\right)^2 + \left(\frac{\partial h_{ave}}{\partial H_{ch}}\delta H_{ch}\right)^2 + \left(\frac{\partial h_{ave}}{\partial T_{w,ave}}\delta T_{w,ave}\right)^2 + \left(\frac{\partial h_{ave}}{\partial T_{f,ave}}\delta T_{f,ave}\right)^2\right]^{\frac{1}{2}} = \left[\left(\frac{\delta q}{q}\right)^2 + \left(\frac{\delta W_s}{W_s}\right)^2 + \left(\frac{\delta W_{ch}}{W_{ch}+2H_{ch}}\right)^2 + \left(\frac{2\delta H_{ch}}{W_{ch}+2H_{ch}}\right)^2 + \left(\frac{\delta T_{w,ave}}{T_{w,ave}-T_{f,ave}}\right)^2 + \left(\frac{\delta T_{f,ave}}{T_{w,ave}-T_{f,ave}}\right)^2\right]^{1/2} \tag{A5}$$

where $q = \dot{V}\rho_{in}c_{p,m}(T_{out}-T_{in})/(W_s L_{ch})$; $\delta q/q$, $\delta T_{w,ave}$ and $\delta T_{f,ave}$ can be calculated by Eq. (A6), Eq. (A7) and Eq. (A8), respectively.

$$\frac{\delta q}{q} = \frac{1}{q}\left[\left(\frac{\partial q}{\partial \dot{V}}\delta \dot{V}\right)^2 + \left(\frac{\partial q}{\partial T_{out}}\delta T_{out}\right)^2 + \left(\frac{\partial q}{\partial T_{in}}\delta T_{in}\right)^2 + \left(\frac{\partial q}{\partial W_s}\delta W_s\right)^2 + \left(\frac{\partial q}{\partial L_{ch}}\delta L_{ch}\right)^2\right]^{\frac{1}{2}} = \left[\left(\frac{\delta \dot{V}}{\dot{V}}\right)^2 + \left(\frac{\delta T_{out}}{T_{out}-T_{in}}\right)^2 + \left(\frac{\delta T_{in}}{T_{out}-T_{in}}\right)^2 + \left(\frac{\delta W_s}{W_s}\right)^2 + \left(\frac{\delta L_{ch}}{L_{ch}}\right)^2\right]^{1/2} \tag{A6}$$

$$\delta T_{w,ave} = \frac{1}{5}\left[\sum_{n=1}^{5}(\delta T_{w,n})^2\right]^{\frac{1}{2}} = \frac{1}{5}\left\{\sum_{n=1}^{5}\left[\left(\frac{\partial T_{w,n}}{\partial T_{R,n}}\delta T_{R,n}\right)^2 + \left(\frac{\partial T_{w,n}}{\partial q}\delta q\right)^2 + \left(\frac{\partial T_{w,n}}{\partial H_R}\delta H_R\right)^2\right]\right\}^{\frac{1}{2}} = \frac{1}{5}\left\{\sum_{n=1}^{5}\left[(\delta T_{R,n})^2 + \left(\frac{H_R}{k_s}\delta q\right)^2 + \left(\frac{q}{k_s}\delta H_R\right)^2\right]\right\}^{1/2} \tag{A7}$$

$$\delta T_{f,ave} = \frac{1}{2}\left[(\delta T_{out})^2 + (\delta T_{in})^2\right]^{1/2} \tag{A8}$$

References

[1] A.F. Al-Neama, Z. Khatir, N. Kapur, J. Summers, H.M. Thompson, An experimental and numerical investigation of chevron fin structures in serpentine minichannel heat sinks, Int. J. Heat Mass Transfer 120 (2018) 1213–1228.
[2] D. Deng, L. Chen, X. Chen, G. Pi, Heat transfer and pressure drop of a periodic expanded-constrained microchannels heat sink, Int. J. Heat Mass Transfer 140 (2019) 678–690.
[3] Z. Feng, X. Luo, F. Guo, H. Li, J. Zhang, Numerical investigation on laminar flow and heat transfer in rectangular microchannel heat sink with wire coil inserts, Appl. Therm. Eng. 116 (2017) 597–609.
[4] M. Ding, C. Liu, Z. Rao, Experimental investigation on heat transfer characteristic of TiO_2-H_2O nanofluid in microchannel for thermal energy storage, Appl. Therm. Eng. 160 (2019) 114024.
[5] C. Xu, S. Xu, S. Wei, P. Chen, Experimental investigation of heat transfer for pulsating flow of GOPs-water nanofluid in a microchannel, Int. Commun. Heat Mass Transfer 110 (2020) 104403.
[6] M. Saeed, M.-H. Kim, Heat transfer enhancement using nanofluids (Al_2O_3-H_2O) in mini-channel heatsinks, Int. J. Heat Mass Transfer 120 (2018) 671–682.
[7] B. Rimbault, C.T. Nguyen, N. Galanis, Experimental investigation of CuO–water nanofluid flow and heat transfer inside a microchannel heat sink, Int. J. Therm. Sci. 84 (2014) 275–292.
[8] G. Liang, I. Mudawar, Review of single-phase and two-phase nanofluid heat transfer in macro-channels and micro-channels, Int. J. Heat Mass Transfer 136 (2019) 324–354.
[9] M. Khoshvaght-Aliabadi, M. Sahamiyan, M. Hesampour, O. Sartipzadeh, Experimental study on cooling performance of sinusoidal–wavy minichannel heat sink, Appl. Therm. Eng. 92 (2016) 50–61.
[10] G. Lu, X. Zhai, Analysis on heat transfer and pressure drop of a microchannel heat sink with dimples and vortex generators, Int. J. Therm. Sci. 145 (2019) 105986.
[11] G. Wang, N. Qian, G. Ding, Heat transfer enhancement in microchannel heat sink with bidirectional rib, Int. J. Heat Mass Transfer 136 (2019) 597–609.

[12] G. Wang, T. Chen, M. Tian, G. Ding, Fluid and heat transfer characteristics of microchannel heat sink with truncated rib on sidewall, Int. J. Heat Mass Transfer 148 (2020) 119142.
[13] M. Sheikholeslami, M. Gorji-Bandpy, D.D. Ganji, Review of heat transfer enhancement methods: Focus on passive methods using swirl flow devices, Renew. Sustain. Energy Rev. 49 (2015) 444–469.
[14] Y. Hong, J. Du, S. Wang, Experimental heat transfer and flow characteristics in a spiral grooved tube with overlapped large/small twin twisted tapes, Int. J. Heat Mass Transfer 106 (2017) 1178–1190.
[15] M.K. Abdolbaqi, W.H. Azmi, R. Mamat, N.M.Z.N. Mohamed, G. Najafi, Experimental investigation of turbulent heat transfer by counter and co-swirling flow in a flat tube fitted with twin twisted tapes, Int. Commun. Heat Mass Transfer 75 (2016) 295–302.
[16] C. Man, X. Lv, J. Hu, P. Sun, Y. Tang, Experimental study on effect of heat transfer enhancement for single-phase forced convective flow with twisted tape inserts, Int. J. Heat Mass Transfer 106 (2017) 877–883.
[17] Y. Hong, J. Du, S. Wang, Turbulent thermal, fluid flow and thermodynamic characteristics in a plain tube fitted with overlapped multiple twisted tapes, Int. J. Heat Mass Transfer 115 (2017) 551–565.
[18] Y. He, L. Liu, P. Li, L. Ma, Experimental study on heat transfer enhancement characteristics of tube with cross hollow twisted tape inserts, Appl. Therm. Eng. 131 (2018) 743–749.
[19] X. Liu, C. Li, X. Cao, C. Yan, M. Ding, Numerical analysis on enhanced performance of new coaxial cross twisted tapes for laminar convective heat transfer, Int. J. Heat Mass Transfer 121 (2018) 1125–1136.
[20] S.M. Abolarin, M. Everts, J.P. Meyer, The influence of peripheral u-cut twisted tapes and ring inserts on the heat transfer and pressure drop characteristics in the transitional flow regime, Int. J. Heat Mass Transfer 132 (2019) 970–984.
[21] S. Zhang, L. Lu, C. Dong, S.H. Cha, Performance evaluation of a double-pipe heat exchanger fitted with self-rotating twisted tapes, Appl. Therm. Eng. 158 (2019) 113770.
[22] S. Zhang, L. Lu, C. Dong, S.H. Cha, Thermal characteristics of perforated self-rotating twisted tapes in a double-pipe heat exchanger, Appl. Therm. Eng. 162 (2019) 114296.
[23] W.X. Chu, C.A. Tsai, B.-H. Lee, K.Y. Cheng, C.-C. Wang, Experimental investigation on heat transfer enhancement with twisted tape having various V-cut configurations, Appl. Therm. Eng. 172 (2020) 115148.
[24] M.M.K. Bhuiya, M.M. Roshid, M.M.M. Talukder, M.G. Rasul, P. Das, Influence of perforated triple twisted tape on thermal performance characteristics of a tube heat exchanger, Appl. Therm. Eng. 167 (2020) 114769.
[25] Y. Hong, J. Du, Q. Li, T. Xu, W. Li, Thermal-hydraulic performances in multiple twisted tapes inserted sinusoidal rib tube heat exchangers for exhaust gas heat recovery applications, Energy Convers. Manag. 185 (2019) 271–290.
[26] M. Sheikholeslami, M. Jafaryar, A. Shafee, Z. Li, R.-u. Haq, Heat transfer of nanoparticles employing innovative turbulator considering entropy generation, Int. J. Heat Mass Transfer 136 (2019) 1233–1240.
[27] S.A. Farshad, M. Sheikholeslami, Nanofluid flow inside a solar collector utilizing twisted tape considering exergy and entropy analysis, Renew. Energy 141 (2019) 246–258.
[28] M. Sheikholeslami, M. Jafaryar, S. Saleem, Z. Li, A. Shafee, Y. Jiang, Nanofluid heat transfer augmentation and exergy loss inside a pipe equipped with innovative turbulators, Int. J. Heat Mass Transfer 126 (2018) 156–163.
[29] M. Sheikholeslami, M. Jafaryar, Z. Li, Nanofluid turbulent convective flow in a circular duct with helical turbulators considering CuO nanoparticles, Int. J. Heat Mass Transfer 124 (2018) 980–989.
[30] M. Sheikholeslami, M. Jafaryar, D.D. Ganji, Z. Li, Exergy loss analysis for nanofluid forced convection heat transfer in a pipe with modified turbulators, J. Mol. Liq. 262 (2018) 104–110.
[31] Z. Li, M. Sheikholeslami, M. Jafaryar, A. Shafee, A.J. Chamkha, Investigation of nanofluid entropy generation in a heat exchanger with helical twisted tapes, J. Mol. Liq. 266 (2018) 797–805.
[32] Z. Feng, X. Luo, J. Zhang, J. Xiao, W. Yuan, Effects of electric field on flow boiling heat transfer in a vertical minichannel heat sink, Int. J. Heat Mass Transfer 124 (2018) 726–741.
[33] S.K. Saha, A. Dutta, S.K. Dhal, Friction and heat transfer characteristics of laminar swirl flow through a circular tube fitted with regularly spaced twisted-tape elements, Int. J. Heat Mass Transfer 44 (22) (2001) 4211–4223.
[34] W. Qu, I. Mudawar, Flow boiling heat transfer in two-phase micro-channel heat sinks—-I. Experimental investigation and assessment of correlation methods, Int. J. Heat Mass Transfer 46 (15) (2003) 2755–2771.
[35] M. Khoshvaght-Aliabadi, M. Sahamiyan, Performance of nanofluid flow in corrugated minichannels heat sink (CMCHS), Energy Convers. Manag. 108 (2016) 297–308.
[36] C.J. Ho, J.C. Liao, W.M. Yan, M. Amani, Experimental study of transient thermal characteristics of nanofluid in a minichannel heat sink with MEPCM layer in its ceiling, Int. J. Heat Mass Transfer 133 (2019) 1041–1051.
[37] M.E. Steinke, S.G. Kandlikar, Single-phase liquid friction factors in microchannels, Int. J. Therm. Sci. 45 (11) (2006) 1073–1083.
[38] R.J. Moffat, Describing the uncertainties in experimental results, Exp. Therm. Fluid Sci. 1 (1) (1988) 3–17.
[39] R.K. Shah, A.L. London, Laminar Flow Forced Convection in Ducts, Academic Press, New York, 1978.
[40] R.J. Phillips, Microchannel Heat Sinks, Advances in Thermal Modeling of Electronic Components and Systems, Hemisphere Publishing Corporation, New York, 1990.
[41] D. Deng, W. Wan, Y. Tang, Z. Wan, D. Liang, Experimental investigations on flow boiling performance of reentrant and rectangular microchannels – A comparative study, Int. J. Heat Mass Transfer 82 (2015) 435–446.
[42] W. Qu, I. Mudawar, Experimental and numerical study of pressure drop and heat transfer in a single-phase micro-channel heat sink, Int. J. Heat Mass Transfer 45 (12) (2002) 2549–2565.
[43] Z.Y. Guo, D.Y. Li, B.X. Wang, A novel concept for convective heat transfer enhancement, Int. J. Heat Mass Transfer 41 (14) (1998) 2221–2225.
[44] H. Safikhani, F. Abbasi, Numerical study of nanofluid flow in flat tubes fitted with multiple twisted tapes, Adv. Powder Technol. 26 (6) (2015) 1609–1617.
[45] Y.L. Zhai, G.D. Xia, X.F. Liu, Y.F. Li, Exergy analysis and performance evaluation of flow and heat transfer in different micro heat sinks with complex structure, Int. J. Heat Mass Transfer 84 (2015) 293–303.
[46] L. Chai, G.D. Xia, H.S. Wang, Parametric study on thermal and hydraulic characteristics of laminar flow in microchannel heat sink with fan-shaped ribs on sidewalls – Part 3: Performance evaluation, Int. J. Heat Mass Transfer 97 (2016) 1091–1101.
[47] J. Zhang, Y. Diao, Y. Zhao, Y. Zhang, Experimental study of TiO_2–water nanofluid flow and heat transfer characteristics in a multiport minichannel flat tube, Int. J. Heat Mass Transfer 79 (2014) 628–638.
[48] C.J. Ho, W.C. Chen, An experimental study on thermal performance of Al_2O_3/water nanofluid in a minichannel heat sink, Appl. Therm. Eng. 50 (1) (2013) 516–522.
[49] S. Ray, A.W. Date, Friction and heat transfer characteristics of flow through square duct with twisted tape insert, Int. J. Heat Mass Transfer 46 (5) (2003) 889–902.
[50] Z. Li, S Khanmohammadi, S. Khanmohammadi, A.A.A.A. Al-Rashed, P. Ahmadi, M. Afrand, 3-E analysis and optimization of an organic rankine flash cycle integrated with a PEM fuel cell and geothermal energy, Int. J. Hydrogen Energy 45 (3) (2020) 2168–2185.